J. Chem, Phys., accepted (2004)

A COMPUTER SIMULATION STUDY OF THE INFLUENCE OF A LIQUID CRYSTAL MEDIUM ON POLYMERIZATION.

Roberto Berardi, Davide Micheletti, Luca Muccioli,

Matteo Ricci, and Claudio Zannoni,

Dipartimento di Chimica Fisica e Inorganica, and INSTM,
Università di Bologna,
Viale Risorgimento 4, 40136 Bologna, Italy.

July 2, 2004

Abstract

We present a simple molecular level model based on Gay–Berne monomers linked by Finitely Extendable Nonlinear Elastic Potential (FENE) bonds for describing main chain polymerization in liquid crystals. We apply the model to study the in uence that the order of the medium has on the characteristics of the chains obtained. We find that the chains prepared from the nematic are actually straighter than those obtained from a polymerization in the isotropic phase and that they are characterized by a small number of hairpins as experimentally observed.

1 Introduction

Main Chain Liquid Crystalline Polymers (MC–LCP) offer a most useful combination of the anisotropy typical of liquid crystal phases and of the mechanical properties typical of polymers.[1–4] A particularly interesting aspect is the possibility of preparing thermotropic MC–LCP with controlled molecular organization and orientational order[2] by polymerization of liquid crystal (LC) monomers started in a suitably ordered phase. Although this has been observed experimentally,[5–7] very little has been done on the modelling side to understand how the anisotropic medium can influence the features of the chains formed through the polymerization process. Here, we tackle the problem by setting up a simple approach to the polymerization in a system of low molar mass LC particles, that we represent at molecular resolution level, and performing Monte Carlo computer simulations starting from isotropic or from nematic phases with different orientational order.[8] Coarse grained polymer models are often of the spherical beads and spring type (see, e.g.[9]), although systems based on ellipsoidal beads have recently been proposed.[10,11] As we shall see our model consists of attractive–repulsive particles that upon polymerization become bonded by flexible linkers. Polymer growth in isotropic monomer melts has been studied by a few authors using lattice[12] and off–lattice[13,14] models but little is known on the influence of solvent anisotropy on the chains formed.

The plan of this paper is as follows: we first describe our molecular model for the monomers, the linkers and the algorithm employed for the simulated polymerization reaction, while in the second part we shall give the Monte Carlo simulation details and describe the results.

2 Model

In the present approach we replace each monomeric LC molecule with an attractive–repulsive Gay–Berne (GB) uniaxial ellipsoid[15] since systems of GB particles have been widely studied as prototype for mesogenic molecules and have been shown to yield the principal thermotropic LC phases (for a recent review see[16]). We are interested in studying the formation of chains and thus we have endowed the GB particles with linking properties so as to model, with small modifications, the two different molecular species we require: monomers and radical initiators.

As monomers link and polymerization takes place, in the way we shall discuss in detail in the following, the total energy of the system will consist of both non–bonded GB terms and of intra–chain terms. Normalizing to the number N of initial monomers in the simulated sample, we can write the energy per particle U as

$$U = U_{GB} + U_{bond}, \tag{1}$$

where U_{GB} and U_{bond} are the non–bonded and bonded interactions energies per particle.

The non–bonded GB interaction term U_{GB} is calculated for all pairs, except for directly linked monomeric units, as

$$U_{GB} = \frac{1}{N}\sum_{i<j}(1 - w_{ij})U_{GB}(\hat{\mathbf{u}}_i, \hat{\mathbf{u}}_j, \mathbf{r}_{ij}), \tag{2}$$

with $\sum_{i<j} = \sum_{i=1}^{N-1}\sum_{j=i+1}^{N}$, and w_{ij} a switch function for bonded monomeric pairs

$$w_{ij} = \begin{cases} 1 & \text{if } i \text{ and } j \text{ are bonded;} \\ 0 & \text{otherwise.} \end{cases} \tag{3}$$

The GB interaction energy between two ellipsoidal particles i, j is given by[15,17]

$$U_{GB}(\hat{\mathbf{u}}_i,\hat{\mathbf{u}}_j, \mathbf{r}_{ij}) = 4\epsilon^{(\mu,\nu)}(\hat{\mathbf{u}}_i, \hat{\mathbf{u}}_j, \hat{\mathbf{r}}_{ij}) \times \left\{ \left[\frac{\sigma_s}{r_{ij} - \sigma(\hat{\mathbf{u}}_i, \hat{\mathbf{u}}_j, \hat{\mathbf{r}}_{ij}) + \sigma_s} \right]^{12} - \left[\frac{\sigma_s}{r_{ij} - \sigma(\hat{\mathbf{u}}_i, \hat{\mathbf{u}}_j, \hat{\mathbf{r}}_{ij}) + \sigma_s} \right]^{6} \right\}, \tag{4}$$

where $\hat{\mathbf{r}}_{ij}$ is a unit vector along the separation vector $\mathbf{r}_{ij}$ joining the centers of mass of particles, i and j, and $\hat{\mathbf{u}}_i$, $\hat{\mathbf{u}}_j$ are unit vectors giving particles orientation. The analytical expression for the interaction strength $\epsilon^{(\mu,\nu)}(\hat{\mathbf{u}}_i, \hat{\mathbf{u}}_j, \hat{\mathbf{r}}_{ij})$ and for the range function $\sigma(\hat{\mathbf{u}}_i, \hat{\mathbf{u}}_j, \hat{\mathbf{r}}_{ij})$, in terms of the long and short axes lengths σ_e, σ_s, and well depths ϵ_e, ϵ_s, as well as the parameters μ, and ν that define the details of the model introduced in refs.[15,16]

Upon bonding, the GB interaction between adjacent pairs of bonded monomers (a.k.a. monomeric units) is replaced by a sum of stretching and bending Finitely Extendable Nonlinear Elastic Potential[18] (FENE) spring contributions, so that the bonded energy per particle term is

$$U_{bond} = \frac{1}{N} \sum_{i<j} w_{ij}[U_s(s_{ij}) + U_\theta(\theta_{ij}) + U_0], \tag{5}$$

where s_{ij} and θ_{ij} are the bond length and angle, as shown in Figure 1. The FENE pair interaction stretching $U_s(s_{ij})$ and bending $U_\theta(\theta_{ij})$ energies between two reaction sites i, j can be written in general terms as[18,19]

$$U_\xi(\xi_{ij}) = -K_\xi \ln \left[1 - \left(\frac{\xi_{ij} - \xi_{eq}}{Q_\xi - \xi_{eq}} \right)^2 \right], \tag{6}$$

where $\xi_{ij} = s_{ij}$ for the stretching, and $\xi_{ij} = \theta_{ij}$ for the bending energy. Here, ξ_{eq} is either the equilibrium bond length s_{eq} or angle θ_{eq}, $K_\xi = \kappa_\xi (Q_\xi - \xi_{eq})^2/2$, where κ_ξ is the force constant, and Q_ξ is the maximum value of bond length or bending angle. If the bond distance and the bending angle are equal to s_{eq} and θ_{eq} respectively, then the pair bonding energy takes the U_0 value. We point out that in the present model the stretching energy does not depend on the orientation of the bond vector $\mathbf{s}_{ij}$ shown in Figure 1 but only on the bond length s_{ij}.

Our algorithm for simulating the polymerization process generalizes the method of Peppas *et al.*[20] to mimic a chain–reaction polymerization (free radical mechanism). We allow bond formation by embedding into each GB monomer two reaction sites, which can exist in three different states: non–bonded, reactive (propagating) and

bonded (see Figure 1). The sites are currently placed in terminal position, although they could be positioned arbitrarily. The model does not involve at the moment a chain–transfer mechanism: consequently the number of growing polymer chains N_c will always be equal to that of radical initiators N_r and, in addition, the propagation reaction is irreversible. Every reaction site can undergo polymerization along a preferential orientation, $\hat{\mathbf{z}}_i^{(1)} = \hat{\mathbf{u}}_i$ for site 1, and $\hat{\mathbf{z}}_i^{(2)} = -\hat{\mathbf{u}}_i$ for site 2.

The polymerization starts with the random generation of a certain number of radical initiators, consisting of monomers carrying a single reacting site. The initiation step is followed by a modified Monte Carlo (MC) evolution, where besides the standard translational and orientational moves[8,21] also reaction steps are performed, during which chain growth moves are attempted. After a successful polymerization event, the non–bonded site of the terminal monomeric unit becomes reactive. The iteration of these steps is continued for a chosen number of MC cycles until the polymerization is quenched. The simulation then continues with the reaction step switched off and the chains are left to evolve and relax for a fixed number of conventional MC simulation cycles during which average properties and observables are computed.

The details of the chain growth process are the following: given the i–th radical with an active terminal site, the monomer most likely to form a new chemical bond is determined by examining its neighbor–list[21] (see Figure 2): only monomers $\{j\}$ with site–site distances s_{ij} and bond angles θ_{ij} falling within certain ranges Δs_m, and $\Delta\theta_m$ from the optimal bond distance s_p and angle θ_p are considered. The monomer chosen for reacting is the one presenting the best (i.e. smallest) value of the merit function

$$\Phi = \frac{|\theta_{ij} - \theta_p|}{\Delta\theta_m} + \frac{|s_{ij} - s_p|}{\Delta s_m}. \tag{7}$$

In Figure 2 we show how the monomer labelled as 2 reacts with the propagating radical 0 as both reaction criteria are satisfied. If no monomer is found the chain propagation does not take place and the propagating radical remains reactive.

3 Computer Simulations

We have simulated, using the MC technique with canonical (NVT) conditions, systems of $N = 4096$ GB monomeric particles in a cubic box with periodic boundaries.[21,22] The parameterization chosen for the GB non–bonded interactions is that already studied in[17] with $\mu = 1$, $\nu = 3$, short axis $\sigma_s = 1\ \sigma_0$, long axis $\sigma_e = 3\ \sigma_0$, and well depths $\epsilon_s = 1\ \epsilon_0$, $\epsilon_e = 0.2\ \epsilon_0$, giving isotropic, nematic and smectic phases at a scaled density $\rho^* = N\sigma_0^3/V = 0.3$ (σ_0 and ϵ_0 are the units of length and energy and if one GB ellipsoid is considered as a typical calamitic mesogen they can be estimated as $\sigma_0 \approx 5 \times 10^{-10}$ m, and $\epsilon_0 \approx 100\ k_B T = 1.38 \times 10^{-21}$ J). In particular, this system has a nematic–isotropic (NI) phase transition at scaled temperature $T^* = k_B T/\epsilon_0 \simeq 3.55$.[17] We have studied the polymerization process by considering systems at various temperatures and with different numbers of radical initiators $N_r = N_c = 10$, 20, 30 corresponding to molar fractions $N_c/N = 2.4 \times 10^{-3}$, 4.9×10^{-3} and 7.3×10^{-3}. Before simulating the chain growth process, the sample of monomeric particles has been equilibrated at each of the three different temperatures studied: $T^* = 2.8$ (nematic), 3.4 (nematic), and 3.8 (isotropic) corresponding to orientational order parameter $\langle P_2 \rangle = 0.81$, 0.63, and 0.04 which, allowing for the larger sample size, is in very good agreement with the values of ref.[17] (also reported in Table 4) for an $N = 1000$ sample. The polymerization reaction (radicals propagation) has been followed for 100 MC kcycles (1 cycle being equal to N attempted MC moves), then polymerization evolution has been stopped, and chains have been left to evolve further for $M = 500$ MC kcycles during which the chains have been allowed to relax. Consequently, the total number of chains N_c and the number of monomeric units in each k–th chain, x_k, used to compute average observables are constant over all M sampled MC configurations. For the chain growth process we have set optimal reaction distance and angle values to $s_p^* = s_p/\sigma_0 = 0.25$, $\theta_p = 180°$, and the maximum deviation ranges to

$\Delta s^*_m = \Delta s_m/\sigma_0 = 0.1$, and $\Delta\theta_m = 90°$. The FENE potential parameters have been set to $s^*_{eq} = s_{eq}/\sigma_0 = 0.15$, $\kappa^*_s = \kappa_s/(\epsilon_0/\sigma_0^2) = 1000$, and $Q^*_s = Q_s/\sigma_0 = 0.4$ for the stretching energy, and $\theta_{eq} = 180°$, $\kappa^*_\theta = \kappa_\theta/\epsilon_0 = 7.6 \times 10^{-4}$ deg^{-2}, and $Q_\theta = 330°$ for the bending energy. Using the approximate conversion factors for σ_0 and ϵ_0 we get $\kappa_s \approx 5.5$ N m^{-1} and $\kappa_b \approx 3.45 \times 10^{-21}$ J rad^{-2}. These values are smaller than the typical stretching and bending terms for a real (e.g. aliphatic) chain, but are appropriate for a molecular model, like the GB one used here, where every FENE bond between GB ellipsoids can be thought as representing a flexible linker joining the mesogenic cores of the MC–LCP. During the MC evolution translational and rotational moves have been attempted on all particles, but chain monomeric units have been selected twice as often to produce a faster chemical bond relaxation.

The specific angular range $\Delta\theta_m$ value of our FENE parameterization allows growing chains to assume a wide range of conformations, so that the polymer structure can be influenced in principle by the LC phase orientational order. In addition, the optimal reaction distance has been chosen to be greater than the FENE bond equilibrium value (i.e. $s_p > s_{eq}$) to increase the number of successful reaction steps. After a reactive event the GB potential is switched off and the bond distance s_{ij} can then relax and assume values closer to s_{eq}. Furthermore, the equilibrium bond distance s_{eq} is smaller than the monomer diameter σ_s, and the stretch constant κ_s has a value preventing the insertion of non reacted monomers between two bonded monomeric units. The remaining FENE parameters have been chosen so that bonded energies do not diverge when FENE interactions are turned on, i.e. $Q_s > |s_p + \Delta s_m|$, and $Q_\theta > |\theta_p + \Delta\theta_m|$. The scalar term U_0 of equation 5 has been put equal to the average non bonded energy $\langle U_{GB}\rangle$ of a monomeric sample at the same temperature T^*, and density ρ^*.[17] In our case we have $U^*_0 = -7.147$ ($T^* = 2.8$), -4.914 ($T^* = 3.4$), and -2.282 ($T^* = 3.8$).

4 Results and Discussion

Turning now to the simulations results, the first fact we wished to asses is if temperature and orientational order do influence the instantaneous monomer conversion $C_{mon} = N_{pol}/N$ during the polymerization process, where $N_{pol} = \sum_x xN(x)$ is the number of reacted monomers, and the length density $N(x)$ counts the number of chains formed by x monomeric units in the sample, so that $N_c = \sum_x N(x)$. In Table 1, and Figure 3 we see that the values of C_{mon} for the nematic phases ($T^* = 2.8$ and 3.4) after the 100 MC polymerization kcycles are quite similar and slightly larger than those obtained in the isotropic sample ($T^* = 3.8$). This effect has been systematically observed during all the polymerization processes studied, and Figure 3 shows that the conversion C_{mon} after a given number of cycles is always lower at the isotropic temperature $T^* = 3.8$. This observation applies to all the polymerization simulations up to the arbitrarily chosen observation length of 100 MC kcycles. The effect of orientational order seems to be that of favoring radicals propagation, which is a reasonable result because ordered monomers are more likely to be found within the useful orientational range from a reaction site as shown in Figure 2. Figure 3 also shows that the chain growth process for the $N_c = 30$ system is linear in the early stages of the reaction whereas it slows down after reaching a conversion $C_{mon} \approx 0.08$. This behavior is visible at all temperatures, also for the $N_c = 10$, and $N_c = 20$ systems.

We now turn to the characterization of the chains formed, particularly with a view to examine the effects, if any, of the onset of ordering in the monomeric system. More in detail, to quantify the elongation and orientational order of the polymer, we have calculated several observables during the sequence of chain relaxation cycles that follow the quenching of the growth reaction. The polymeric chains distribution has been characterized by computing a few observables[23] normally

used for this purpose, i.e. the number–average degree of polymerization

$$\bar{x}_n = N_{pol}/N_c, \tag{8}$$

and the weight–average degree of polymerization

$$\bar{x}_w = \frac{1}{N_{pol}} \sum_x x^2 N(x). \tag{9}$$

The average values of the two degrees of polymerization observed for our model systems are reported in Table 1. We find that for all values of N_c studied the chains become on average longer (i.e. with larger $\bar{x}_n$, and $\bar{x}_w$) as temperature decreases and order increases. This is again consistent with a higher probability of successful MC reactive moves in the low–temperature systems where the orientational order favors the growing of chains before the reaction is quenched. Furthermore, the system with lowest number of propagating radicals exhibits the longest chains, because of the higher concentration of monomers in the neighborhood of the propagating sites during the polymerization process. Given the limited number of chains in our MC samples the computation of the moments of $N(x)$ does not give a very high statistical accuracy and it is not possible to draw further conclusions from the analysis of the degrees of polymerization.

We have also calculated chain observables and examined their dependence from the temperature and orientational order. The first one we take into account is the average end–to–end distance

$$\langle r_{ee} \rangle = \frac{1}{M N_c} \sum_{m=1}^{M} \sum_{k=1}^{N_c} r_{ee}^{(m,k)}, \tag{10}$$

where $r_{ee}^{(m,k)}$ is the distance between the tips of the first and last monomeric units in the k–th chain for the m–th MC configuration. The end–to–end distances are strictly correlated to chain structure and have showed only small variations during the relaxation run. This behavior suggests that when the polymerization reaction is stopped the polymeric chains properties fluctuate around their average values.

The effect of orientational order is clearly given by the ratios $\langle r_{ee}\rangle/r_m$ reported in Table 2. We see that in the nematic samples at the lowest temperature ($T^* = 2.8$) the $\langle r_{ee}\rangle$ distances are more than 90% of the contour length $r_m = s_{eq}(\bar{x}_n - 1) + \sigma_e \bar{x}_n$, i.e. of the limiting length of a fully stretched chain of the same length $\bar{x}_n$. The ratio $\langle r_{ee}\rangle/r_m$ decreases only a few units percent if we go from $T^* = 2.8$ to the highest nematic temperature $T^* = 3.4$ (with $\Delta T^* = 0.6$) while, moving further to the isotropic case, $T^* = 3.8$, this decrease roughly becomes $10 - 20\%$ (for a $\Delta T^* = 0.4$). Nonetheless, in the isotropic sample at $T^* = 3.8$ this ratio is still quite high and the $\langle r_{ee}\rangle$ distance is much larger than the value $\langle r_{ee}\rangle_{rc} \approx (s_{eq} + \sigma_e)\bar{x}_n^{1/2}$ expected for a random coil formed by $\bar{x}_n$ freely jointed units[23] of length $s_{eq} + \sigma_e$; this is a consequence of the monomer shape and of the chain intrinsic stiffness. Finally, we see that the ratio $\langle r_{ee}\rangle/r_m$ is not affected by the number of radical initiators.

One possible way to asses polymer stiffness is to analyze the average deviations from equilibrium values of bond lengths s_{eq}, and bending angles θ_{eq} namely, $\Delta s = \langle (s_{ij} - s_{eq})^2\rangle^{1/2}$, and $\Delta\theta = \langle (\theta_{ij} - \theta_{eq})^2\rangle^{1/2}$. The values obtained for our model systems are reported in Table 3, and we see that bond length fluctuations Δs slightly decrease with temperature, as one would expect. This can be interpreted in terms of the value of κ_s, which makes bonds rather stiff with respect to the scale of GB interactions: on average we find that at all temperatures the fluctuations are ≈ 20 % of the amplitude of the FENE potential range around s_{eq}. Our choice of κ_b results instead in a wider fluctuation range of bending angles as it is apparent from the $\Delta\theta$ values reported in Table 3. The effect of temperature is in this case more pronounced and in the isotropic sample we observe a $\Delta\theta \approx 70^\circ$, while in the nematic systems the average deviations from θ_{eq} become considerably smaller (by a factor $1.5 - 2$), which is an evident effect of temperature and orientational disorder on chains structure. We do not observe any apparent effect due to the propagating radical concentration and the data for the $N_c = 20$, $N_c = 30$ systems

are the same as those for the $N_c = 10$ case reported in Table 3.

Moving to the description of the anisotropic properties of the samples, the orientational order of the polymeric chain can be referred to the global mesophase director or to a specific molecular axis and here we have considered both. The global second rank orientational order parameter $\langle P_2^{(d)} \rangle$ is relative to all N anisotropic beads (i.e. bonded and non–bonded monomers) and it is referred to the phase director $\hat{\mathbf{d}}^{(m)}$, computed in the standard fashion by diagonalization of the ordering matrix[24]

$$\langle P_2^{(d)} \rangle = \frac{1}{MN} \sum_{m=1}^{M} \sum_{i=1}^{N} P_2 \left[\hat{\mathbf{u}}_i^{(m)} \cdot \hat{\mathbf{d}}^{(m)} \right], \tag{11}$$

where $\hat{\mathbf{u}}_i^{(m)}$ is the orientation of the i–th monomer in the m–th configuration, and $P_2 \left[\hat{\mathbf{u}}_i^{(m)} \cdot \hat{\mathbf{d}}^{(m)} \right] = (3\cos^2 \beta_i - 1)/2$, where $\cos \beta_i = \hat{\mathbf{u}}_i^{(m)} \cdot \hat{\mathbf{d}}^{(m)}$. An additional order parameter $\langle P_2^{(e)} \rangle$, describing the average alignment of each monomeric unit $\hat{\mathbf{u}}^{(m,k)}$ with respect to the chain axis $\hat{\mathbf{e}}^{(m,k)}$ has also been computed as

$$\langle P_2^{(e)} \rangle = \frac{1}{MN_c} \sum_{m=1}^{M} \sum_{k=1}^{N_c} \frac{1}{x_k} \sum_{l=1}^{x_k} P_2 \left[\hat{\mathbf{u}}_l^{(m,k)} \cdot \hat{\mathbf{e}}^{(m,k)} \right], \tag{12}$$

where every chain axis $\hat{\mathbf{e}}^{(m,k)}$ has been determined as the eigenvector of the chain inertial tensor corresponding to the lowest eigenvalue. The orientational order parameters for the $N_c = 10$ systems are reported in Table 4, and we see that the average value of $\langle P_2^{(e)} \rangle$ is practically coincident with $\langle P_2^{(d)} \rangle$ at all temperatures. Furthermore, in the nematic phases $\langle P_2^{(d)} \rangle$ is only slightly higher than the $\langle P_2 \rangle$ obtained for the bulk system of $N = 1000$ GB particles of ref.[17] Thus, the effect of chains in further promoting the orientational alignment of the nematic solvent seems negligible in our samples and the differences between $\langle P_2^{(d)} \rangle$ and $\langle P_2 \rangle$ in Table 4 may also originate from the different sample sizes of this work ($N = 4096$) and that of ref.[17] Moreover we find that for the order parameters there is no influence from the number of radicals and results for the $N_c = 20$, $N_c = 30$ systems are the same as those for the $N_c = 10$ case reported in Table 4.

Finally, we have monitored orientational pair correlations along the polymeric

chains. They have been computed starting from the instantaneous $C_2^{(m,k)}(n)$ functions

$$C_2^{(m,k)}(n) = \frac{1}{N_k - n} \sum_{l=1}^{N_k - n} P_2 \left[\hat{\mathbf{u}}_l^{(m,k)} \cdot \hat{\mathbf{u}}_{l+n}^{(m,k)} \right], \tag{13}$$

relative to pairs n units apart in the k–th chain and m–th MC configuration. The overall average correlation function $\langle C_2(n) \rangle$ has been obtained by summing all separate chain contributions, and by normalizing with respect to the total number of chains and MC configurations analyzed

$$\langle C_2(n) \rangle = \frac{1}{M N_c} \sum_{m=1}^{M} \sum_{k=1}^{N_c} C_2^{(m,k)}(n). \tag{14}$$

The correlation function profiles $\langle C_2(n) \rangle$ at the various temperatures range from 1 for $n = 0$ (short–range) to an asymptotic value $\langle P_2^{(d)} \rangle^2$ for $n \to \infty$ (long–range). Since $\langle P_2^{(d)} \rangle$ essentially corresponds to the order of the monomeric particles, the influence of the phase anisotropy to the structure of polymeric chains can be studied by looking at this observable. Furthermore, an analysis of the first portion of the $\langle C_2(n) \rangle$ profiles gives information on the short–range orientational order around a monomeric unit. The plots shown in Figure 4 are for the $N_c = 10$ systems but are representative of all radicals concentration cases we have studied. The nematic sample at highest order parameter $\langle P_2^{(d)} \rangle = 0.81$ (and $T^* = 2.8$) presents the largest starting value for $n = 1$ which quickly lowers to the asymptotic value indicating that the monomeric units are highly correlated for all intra–chain separations. This is consistent with the fact that the chains are fairly linear. In the nematic sample with $\langle P_2^{(d)} \rangle = 0.67$ at $T^* = 3.4$ the pair correlation has a slightly larger jump between short– and long–range values (the overall orientational order is smaller) but again it levels to the asymptotic limit just after two or three monomeric units. In the isotropic phase at $T^* = 3.8$ and $\langle P_2^{(d)} \rangle = 0.03$ the chains are on average disordered and the asymptotic limit is $\langle P_2^{(d)} \rangle^2 = 0$. Nonetheless, the short–range portion of the curve is not zero and approaches the long–range limit in a slightly slower fashion (after 7, 8 monomeric units) than in the nematic

phases. This indicates that, in spite of the bending constant being fairly small and chains quite flexible, there is still some local coherence of the units.

Examining the snapshots of Figure 5 relative to the beginning of the polymerization reactions of systems with radical concentration $N_c = 30$, we see that the chain structure is indeed influenced by the orientational order: in the lowest temperature nematic sample ($T^* = 2.8$) chains are fairly elongated, and at $T^* = 3.4$ they become less aligned, while in the isotropic phase ($T^* = 3.8$) structures are disordered but still not densely packed as a random–coil. This is reasonable because the polymer is soluble in the monomers solution and there is no evidence of segregation. The features of these structures can be more easily seen if we unwind the periodic boundaries and show only one polymeric strand. In Figure 6 we show a sequence of three snapshots of a single growing chain for the $T^* = 2.8$, and $T^* = 3.8$ samples after 20, 60, and 100 MC kcycles where the differences are quite evident. If we compare what emerges from our data, shown in Table 4 and Figure 4, with the results of Lub *et al.*[7] we find that the conclusions drawn by analyzing the correlations functions are consistent with that experimental work: a polymerization reaction performed in a suitable liquid crystalline monomer solution results in the formation of chains whose structure is a function of the orientational order.

Although polymers formed from the nematic melt are more straight it is important to see if chains can anyway occasionally bend on themselves, forming sharp *"u–turns"*, the so–called hairpins. These have been observed experimentally at least in some main chain polyesters[25] and polyethers.[26] In the remaining part of this paper we discuss the analyses we have performed on chain structures after the relaxation runs have finished, to observe if one or more bends were present. The operational definition we have used for a hairpin in a polymeric chain is the following: the shortest chain portion whose first and last monomeric units i, j exhibit a value of $P_1(\hat{\mathbf{u}}_i \cdot \hat{\mathbf{u}}_j) = \cos\beta_{ij} \leq \cos\theta_{hp}$, where $\cos\beta_{ij} = \hat{\mathbf{u}}_i \cdot \hat{\mathbf{u}}_j$. The hairpin threshold angle has been chosen $\theta_{hp} = 160°$ (see Figure 7 for a pictorial representation),

and two additional constraints have been enforced to avoid overlapping hairpins and considering wide bends: neither i and j must be within another pin, and $i < j \leq i + 5$, so that the maximal hairpin length is 6 units, and any u–turn involving more than 6 monomeric units is not considered here as a pin.

In Table 1 we also report the number N_{cp} of chains showing one ore more hairpins upon completion of the 500 kcycles relaxation run. We see that for all concentrations of initiators only $5 - 10\%$ of the total number of chains N_c at the nematic temperature $T^* = 2.8$ have an u–turn. This number increases to $20 - 40\%$ moving to the $T^* = 3.4$ systems where the lower orientational order gives access to the newly forming bonds to larger fluctuations in bending angle. Finally, the number N_{cp} slightly decreases in the isotropic phase at $T^* = 3.8$ since sharp u–turns are now less probable because of the high chain flexibility which also favors chain loops with larger curvature radiuses. We have estimated the average number of hairpins N_{hp} with respect to the N_{cp} chains with one or more conformational u–turns, finding that on average there is only one hairpin per bent chain, and that N_{cp} increases with temperature in the nematic phase. Interestingly this is similar to what was observed experimentally[26] and it is understandable as hairpins only determine a local perturbation in the system without affecting the overall orientational ordering of the system. In our case, the average length of such hairpins L_{hp} is four monomeric units.

5 Conclusions

We have developed a Gay–Berne model to describe a polymerization process in a condensed, isotropic or liquid crystalline phase and a set of tools for the characterization of the chains obtained. The Monte Carlo simulations have shown that, if the chains are flexible, the polymerization of a monomer in a nematic phase gives rise to a polymer with an orientational order similar to that of the liquid crystal

phase. In this case the order of the medium does influence both the growth and the structure of the polymeric chains. The possibility of generating well ordered macromolecules from low molar mass monomers, as we have discussed, offers a powerful way of controlling the orientational persistence properties of polymers. We have also studied the appearance of hairpins and we have found that, in agreement with experiment, they are not completely forbidden. On the whole, the Gay–Berne model originally developed for low molecular weight liquid crystalline systems can thus be employed for studying polymer melts.

Acknowledgements

We thank MIUR (PRIN *"Cristalli Liquidi"*), EU (TMR FULCE *"Functional Liquid–Crystalline Elastomers"*, contract HPRN-CT-2002-00169), INSTM, and University of Bologna for financial support.

References

[1] A. M. Donald and A. H. Windle, *Liquid Crystalline Polymers* (Cambridge University Press, Cambridge, 1992).

[2] A. A. Collyer, Materials Science and Technology **5**, 309 (1989).

[3] G. Vertogen and W. H. de Jeu, *Thermotropic Liquid Crystals, Fundamentals* (Springer–Verlag, Berlin, 1988).

[4] A. A. Collyer, Materials Science and Technology **6**, 984 (1990).

[5] D. J. Broer and G. N. Mol, ACS Symposium Series **346**, 417 (1987).

[6] D. J. Broer, H. Finkelmann and K. Kondo, Makromolekulare Chemie **189**, 185 (1988).

[7] J. Lub, D. J. Broer, M. E. Martinez Antonio and G. N. Mol, Liq. Cryst. **24**, 375 (1998).

[8] P. Pasini and C. Zannoni, editors, *Advances in the Computer Simulations of Liquid Crystals* (Kluwer Academic Publishers, Dordrecht, 2000).

[9] K. Binder, editor, *Monte Carlo and Molecular Dynamics Simulations in Polymer Science* (Oxford University Press, Oxford, 1995).

[10] A. V. Lyulin, M. S. Al-Barwani, M. P. Allen, M. R. Wilson, I. Neelov and N. K. Allsopp, Macromolecules **31**, 4626 (1998).

[11] O. Hahn, L. Delle Site and K. Kremer, Macromol. Theory Simul. **10**, 288 (2001).

[12] M. Vogt and R. Hernandez, J. Chem. Phys. **116**, 10485 (2002).

[13] R. L. C. Akkermans, S. Toxvaerd and W. J. Briels, J. Chem. Phys. **109**, 2929 (1998).

[14] S. Toxvaerd, J. Mol. Liq. **84**, 99 (2000).

[15] J. G. Gay and B. J. Berne, J. Chem. Phys. **74**, 3316 (1981).

[16] C. Zannoni, J. Mater. Chem. **11**, 2637 (2001).

[17] R. Berardi, A. P. J. Emerson and C. Zannoni, J. Chem. Soc. Faraday Trans. **89**, 4069 (1993).

[18] R. B. Bird, R. C. Armstrong and D. Hassager, *Dynamics of Polymeric Liquids* (J. Wiley, New York, 1971).

[19] R. S. Khare, J. J. de Pablo and A. Yethiraj, Macromolecules **29**, 7910 (1996).

[20] D. L. Kurdikar, H. M. J. Boots and N. A. Peppas, Macromolecules **28**, 5632 (1995).

[21] M. P. Allen and D. J. Tildesley, *Computer Simulation of Liquids* (Oxford University Press, Oxford, 1989).

[22] D. Frenkel and B. Smit, *Understanding Molecular Simulations: From Algorithms to Applications* (Academic Press, San Diego, 1996).

[23] P. J. Flory, *Principles of Polymer Chemistry* (Cornell University Press, Ithaca, 1953).

[24] C. Zannoni, in *The Molecular Physics of Liquid Crystals*, edited by G. R. Luckhurst and G. W. Gray, chap. 3, 51–83 (Academic Press, London, 1979).

[25] M. Li, A. Brûlet, P. Davidson, P. Keller and J. P. Cotton, Phys. Rev. Lett. **70**, 2297 (1993).

[26] F. Hardouin, G. Sigaud, M. F. Achard, A. Brûlet, J. P. Cotton, D. Y. Yoon, V. Percec and M. Kawasumi, Macromolecules **28**, 5427 (1995).

	$N_c = 10$			$N_c = 20$			$N_c = 30$		
T^*	2.8	3.4	3.8	2.8	3.4	3.8	2.8	3.4	3.8
C_{mon}	0.22	0.21	0.18	0.34	0.34	0.31	0.42	0.42	0.40
$\bar{x}_n$	90	84	74	69	70	63	58	57	55
$\bar{x}_w$	93	85	76	72	72	64	61	59	61
N_{cp}	1	4	4	1	4	2	2	11	8

Table 1: The monomer conversion C_{mon}, the average degrees of polymerization $\bar{x}_n$, $\bar{x}_w$ for all radicals concentrations after the 100 kcycles MC polymerization process, and the number N_{cp} of chains showing at the end of the 500 kcycles relaxation run one or more hairpins.

	T^*	$\langle r^*_{ee} \rangle$	r^*_m	$\langle r^*_{ee} \rangle / r^*_m$	$\langle r^*_{ee} \rangle_{rc}$
$N_r = 10$	2.8	259.3 ± 0.4	283.4	0.92	29.8
	3.4	234.5 ± 0.4	264.4	0.89	28.9
	3.8	184.1 ± 1.0	233.0	0.79	27.1
$N_r = 20$	2.8	198.6 ± 0.2	217.2	0.91	26.2
	3.4	194.7 ± 0.3	220.4	0.88	26.4
	3.8	158.2 ± 0.6	198.3	0.80	25.0
$N_r = 30$	2.8	167.1 ± 0.2	182.6	0.92	23.4
	3.4	160.0 ± 0.2	179.4	0.89	23.8
	3.8	138.1 ± 0.4	173.1	0.80	23.4

Table 2: The average dimensionless end–to–end distances $\langle r^*_{ee} \rangle$ after the 500 kcycles MC chain relaxation process described in the text. The dimensionless ideal contour length for a fully stretched chain r^*_m of length $\bar{x}_n$, and the end–to–end distance for a freely jointed chain $\langle r^*_{ee} \rangle_{rc}$ discussed in the text are also reported.

T^*	Δs^*	$\Delta s/\lvert Q_s - s_{eq}\rvert$	$\Delta\theta/^\circ$	$\Delta\theta/\lvert Q_\theta - \theta_{eq}\rvert$
2.8	0.054 ± 0.001	0.22	28 ± 5	0.19
3.4	0.059 ± 0.001	0.24	42 ± 7	0.28
3.8	0.062 ± 0.001	0.25	69 ± 8	0.46

Table 3: The dimensionless average deviations Δs^*, and $\Delta\theta$ from FENE equilibrium values for the relaxed $N_c = 10$ chains described in the text. Ratios are normalized with respect to FENE maximum deviations, $|Q_s - s_{eq}| = 0.25\ \sigma_0$ and $|Q_\theta - \theta_{eq}| = 150^\circ$. The values of deviations Δs^* and $\Delta\theta$ for the $N_c = 20$, and $N_c = 30$ systems are the same as the $N_c = 10$ case.

T^*	$\langle P_2^{(d)} \rangle$	$\langle P_2^{(e)} \rangle$	$\langle P_2 \rangle$
2.8	0.81 ± 0.01	0.82 ± 0.01	0.80 ± 0.02
3.4	0.67 ± 0.01	0.68 ± 0.02	0.63 ± 0.03
3.8	0.03 ± 0.01	0.04 ± 0.01	0.10 ± 0.04

Table 4: The second rank order parameters $\langle P_2^{(d)} \rangle$ and $\langle P_2^{(e)} \rangle$ for the relaxed $N_c = 10$ polymeric chains. The order parameters $\langle P_2 \rangle$ for the system of $N = 1000$ GB particles of ref.[17] are also reported for comparison. The values of order parameters for the $N_c = 20$ and $N_c = 30$ systems are the same as those for the $N_c = 10$ case.

List of Figures

Figure 1: Schematic drawing of a bonded monomeric particle i with orientation vector $\hat{\mathbf{u}}_i$ and reaction sites #1, and #2 with orientations $\hat{\mathbf{z}}_i^{(1)} = -\hat{\mathbf{z}}_i^{(2)}$, and positions (0, 0, d), and (0, 0, $-d$), where $d = \sigma_e/2$. The site–site vector $\mathbf{s}_{ij}$ and the bending angle θ_{ij} between the bonded $\hat{\mathbf{z}}_i^{(1)}$ and $\hat{\mathbf{z}}_j^{(2)}$ sites are also shown. The active propagating site $\hat{\mathbf{z}}_j^{(1)}$ is shown as a circular outline, while the dashed particle on the left represents the remaining part of the chain.

Figure 2: Cartoon describing the positional (a) and orientational (b) criterions used to select candidate monomers for the MC chain propagation reaction. Monomer #2 may react with propagating radical #0 since both reaction criterions are fulfilled: the bond distance $s_p - \Delta s_m \leq s_{02} \leq s_p + \Delta s_m$, and bending angle $\theta_p - \Delta\theta_m \leq \theta_{02} \leq \theta_p + \Delta\theta_m$ are within the useful ranges for a bonding reaction. On the other hand, monomer #1 only fulfills the angular criterion, while monomer #3 only satisfies the distance criterion.

Figure 3: The MC evolution of the instantaneous monomer conversion C_{mon} for the $N_c = 30$ system during the polymerization reaction at the three temperatures studied.

Figure 4: The average correlation function $\langle C_2(n) \rangle$ for the $N_c = 10$ system computed during the 500 kcycles MC chain relaxation.

Figure 5: Snapshots of the $N_c = 30$ MC systems at the three temperatures studied taken in the early stages of the polymerization reaction (after 10 MC kcycles). The terminal propagating monomeric units are colour coded as dark gray particles.

Figure 6: Sequences of snapshots of a growing polymeric chain at $T^* = 2.8$ (nematic: a, b, c) and $T^* = 3.8$ (isotropic: d, e, f) for the $N_c = 30$ system, after 20 (a, d), 60 (b, e), and 100 (c, f) MC kcycles of the polymerization reaction. The terminal active monomer is represented as a dark gray ellipsoid. To help the visualisation, chains have been unwounded from the MC periodic boundary conditions.

Figure 7: The representation of a polymeric chain showing a pair of hairpins 4, and 5 monomeric units long (a). The starting and terminal particles defining the pins are shaded and joined with a light gray line. Snapshots of two chains with hairpins in the nematic samples at $T^* = 2.8$ (b, 64 units), and $T^* = 3.4$ (c, 49 units) for the $N_c = 30$ system. To help in the visualisation, chains have been unwounded from the MC periodic boundaries.

Figure 1

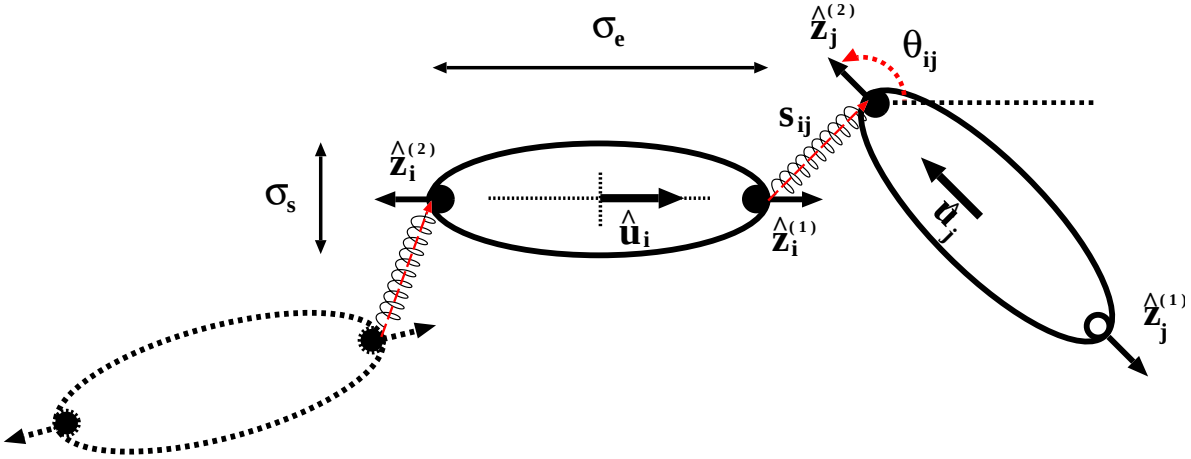
σ_e
$\hat{z}_j^{(2)}$
θ_{ij}
s_{ij}
σ_s
$\hat{z}_i^{(2)}$
$\hat{u}_i$
$\hat{z}_i^{(1)}$
$\hat{u}_j$
$\hat{z}_j^{(1)}$

Figure 2

(a)

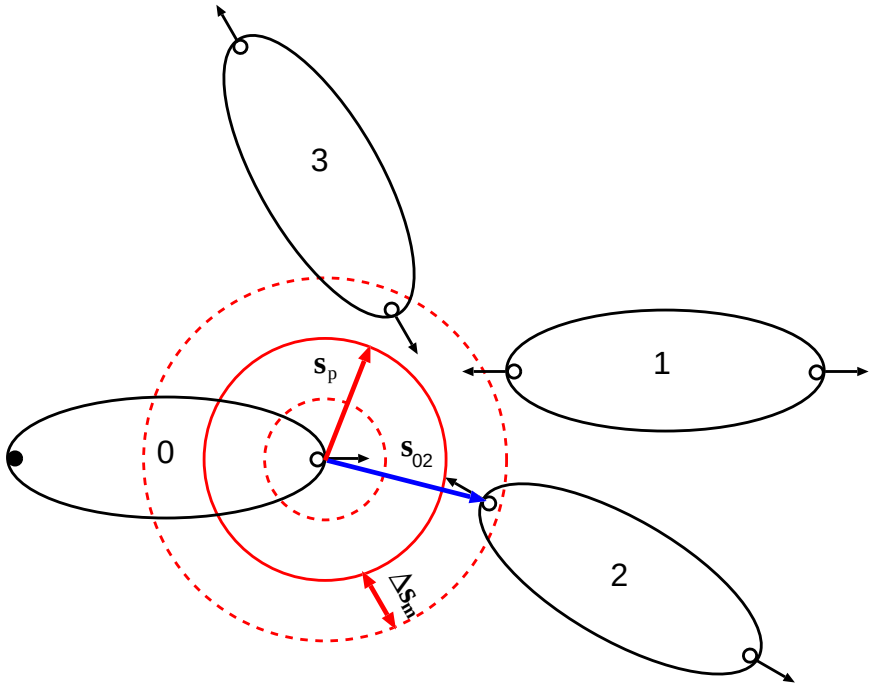
3
1
0
2
$\mathbf{s}_p$
$\mathbf{s}_{02}$
Δs_m

(b)

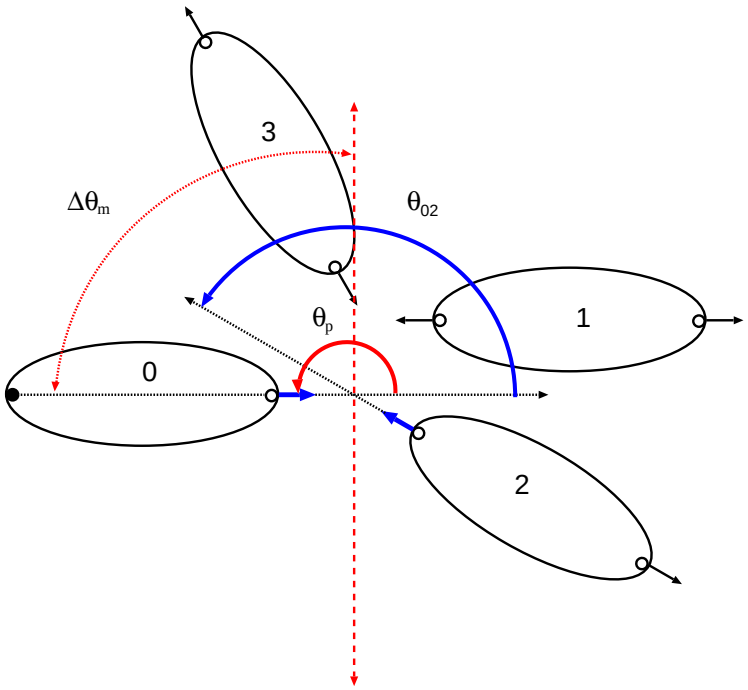
3
1
0
2
$\Delta\theta_m$
θ_{02}
θ_p

Figure 3

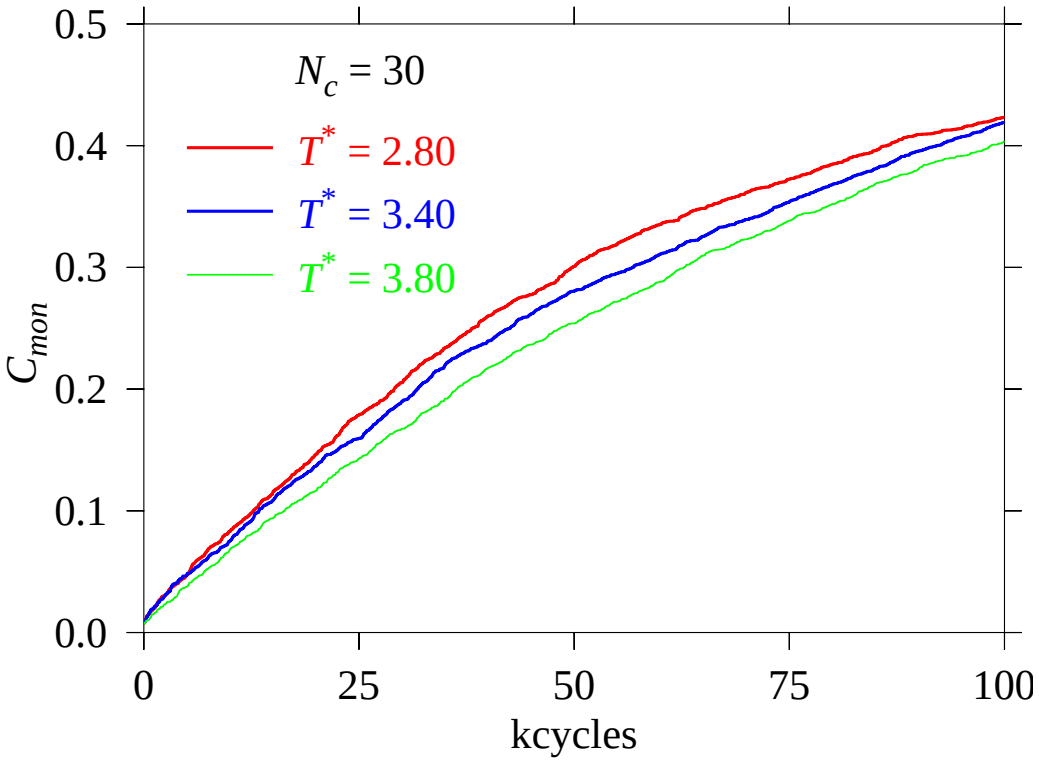

Figure 4

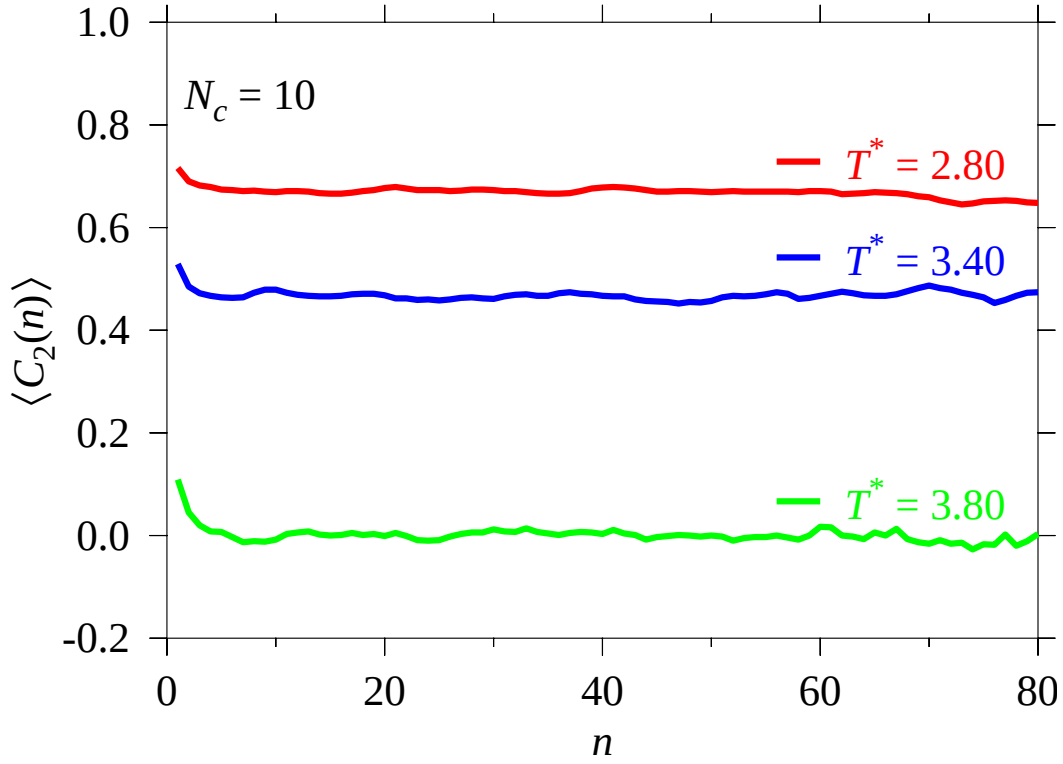
1.0
0.8
0.6
0.4
0.2
0.0
-0.2
0
20
40
60
80
$\langle C_2(n) \rangle$
n
N_c = 10
T^* = 2.80
T^* = 3.40
T^* = 3.80

Figure 5

(a) $T^* = 2.8$, $C_{mon} = 0.08$

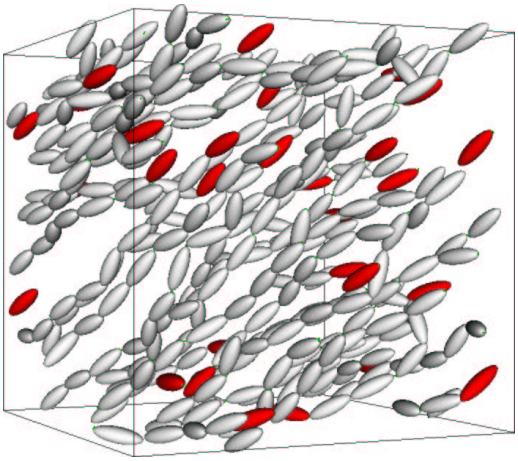

(b) $T^* = 3.4$, $C_{mon} = 0.07$

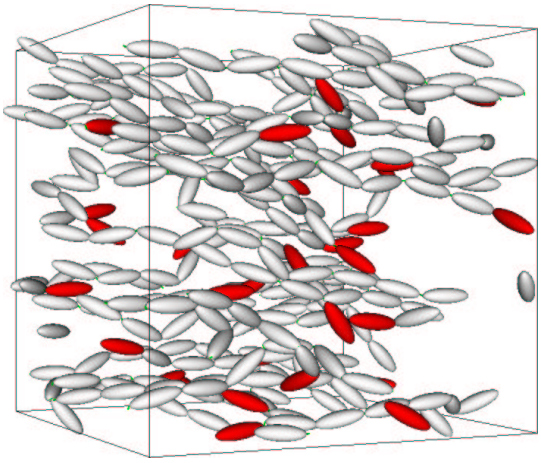

(c) $T^* = 3.8$, $C_{mon} = 0.06$

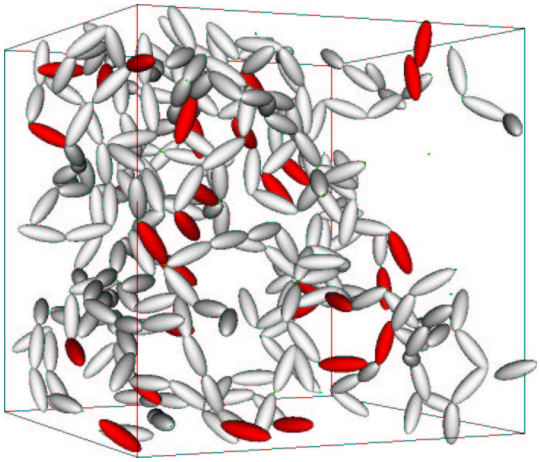

Figure 6

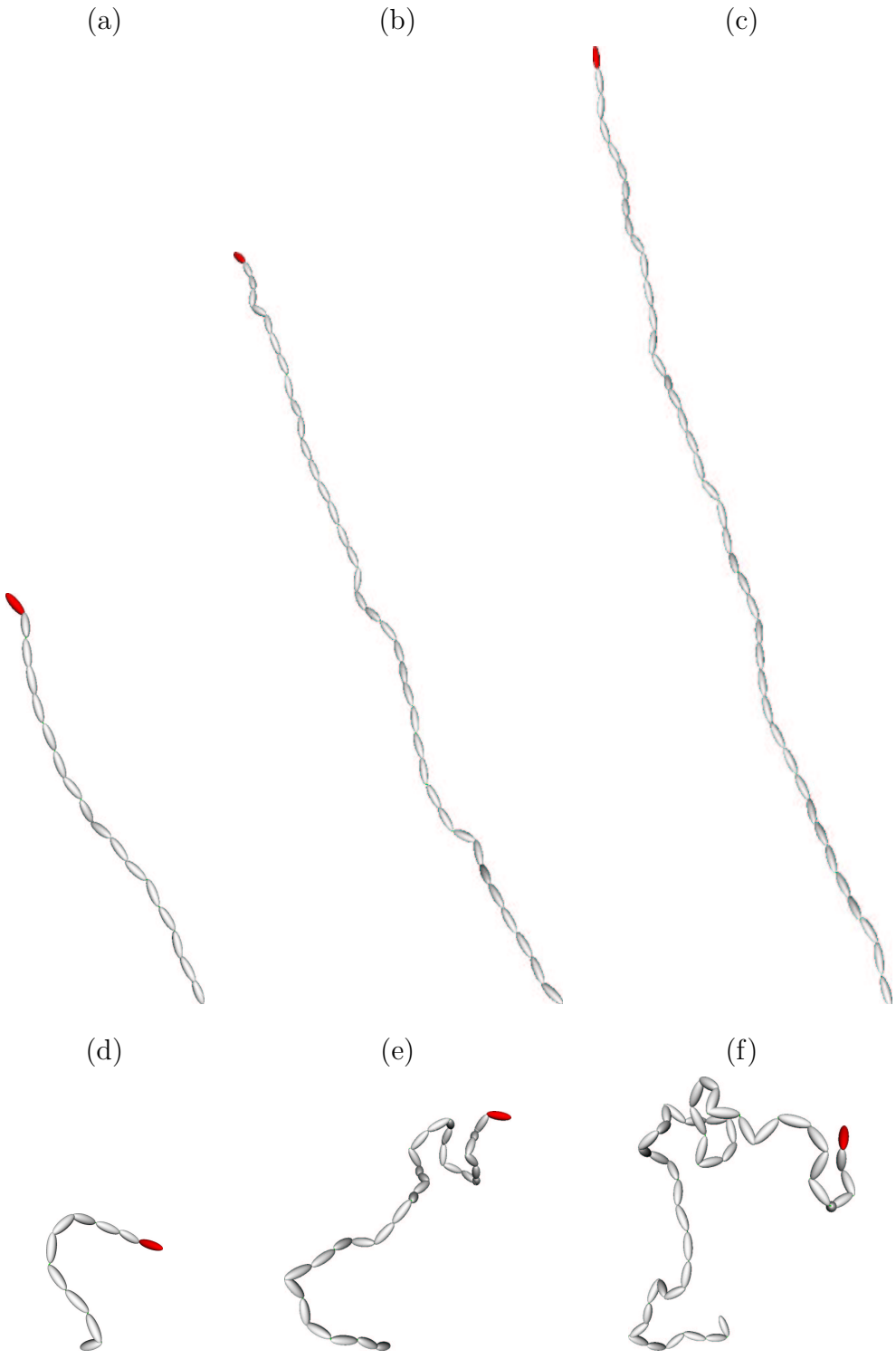

Figure 7

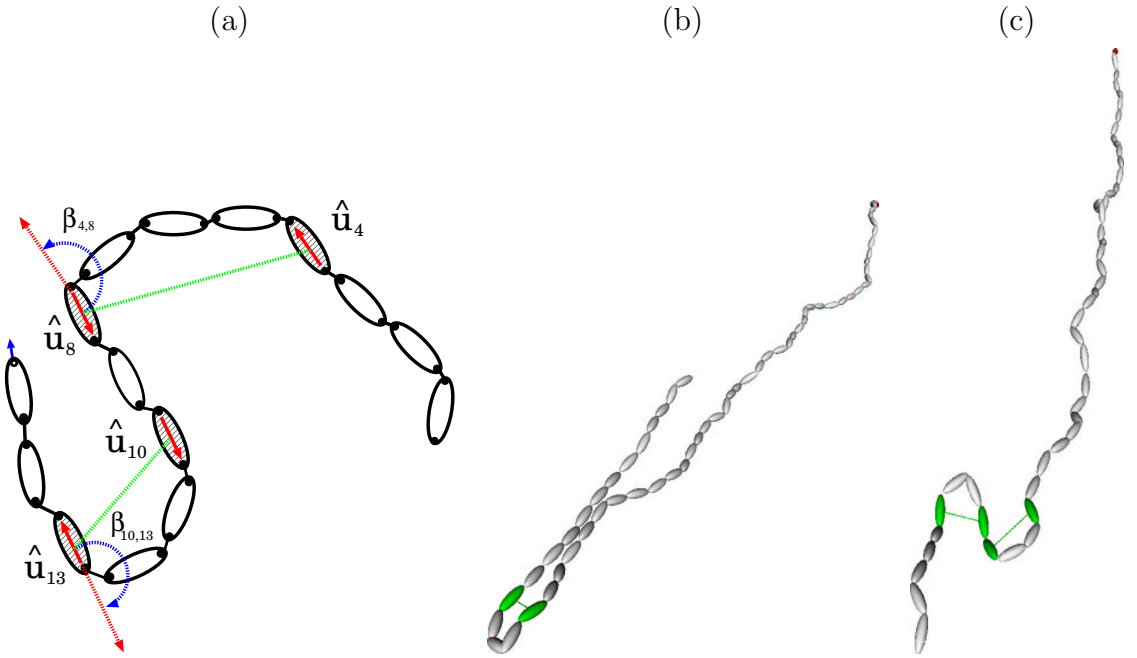
(a)
(b)
(c)
$\beta_{4,8}$
$\hat{\mathbf{u}}_4$
$\hat{\mathbf{u}}_8$
$\hat{\mathbf{u}}_{10}$
$\beta_{10,13}$
$\hat{\mathbf{u}}_{13}$